ELSEVIER

Journal of Nuclear Materials 264 (1999) 113–121

journal of nuclear materials

A model of silver–iodine reactions in a light water reactor containment sump under severe accident conditions

Elisabeth Krausmann *, Yannis Drossinos

European Commission, Joint Research Centre, via E. Fermi 1, I-21010 Ispra (VA), Italy

Received 7 April 1998; accepted 2 July 1998

Abstract

Metallic silver and iodine form insoluble AgI in the containment sump which has a major impact on iodine volatility and hence on the source term to the environment. Resistance-in-series models are developed and validated against separate-effects tests. The reaction between I_2 and Ag is limited by mass transfer in the liquid. The rate does not follow a parabolic law for the duration of the experiments. The extent of oxidation of the silver sample seems to play a decisive role for reactions with I^- which proceed via a two-step process. The initial, rapid step is controlled by the reaction with the surface silver oxide with a contribution of mass transfer in the liquid. The subsequent, slow step is limited by reaction between I^- and Ag^+ at the solid–liquid interface. The reaction is probably negligible for pH > 7 and in the absence of oxidising conditions.

1. Introduction

In the case of a loss-of-coolant accident in a nuclear power plant the temperature rise would lead to substantial failure of the fuel rods giving rise to a release of fission products into the primary circuit and eventually into the containment. Knowledge of the behaviour of radioactive fission products is essential for the prediction of the source term to the environment during a severe accident. The behaviour of radioiodine is of special interest as it forms volatile compounds which are difficult to contain in the case of a containment leak and due to its biological activity that poses a cancer risk after accumulation in the thyroid gland.

In a severe accident the silver–indium–cadmium control rods usually employed in Light Water Reactors (LWR) would also fail due to the prevailing high temperatures causing the release of silver, indium and cadmium. Results of the first test FPT-0 of the Phebus-FP programme [1] and new studies on the effect of silver on iodine volatility [2–4] suggest that the presence of a large amount of silver has a major impact on the volatility of iodine from solution. The reaction of silver (Ag) with either water-soluble iodide (I^-) or dissolved molecular iodine (I_2) leads to the formation of silver iodide (AgI), which is non-volatile and has a very low solubility in water [3]. Provided that AgI withstands radiolytic decomposition it represents a permanent iodine sink and reduces the amount of volatile iodine present in the containment atmosphere.

The behaviour of iodine observed in FPT-0 and that predicted by containment chemistry simulations differs considerably indicating that current models do not satisfactorily treat relevant reactor accident phenomena. In particular, models for the reaction of Ag with I and its consequences on iodine volatility under severe accident conditions have to be developed and validated against experimental data and then included into iodine codes.

In this work we propose a model that describes the reaction between Ag and I and which incorporates transport phenomena, i.e. mass transport in the liquid and the solid phase, as well as the chemical reaction at the reaction interface, considering these processes as 'resistances in series'.

2. Experimental basis

The model to be developed in this work is based on separate-effects tests performed by AEA Technology

* Corresponding author.

0022-3115/99/$ – see front matter
PII: S0022-3115(98)00471-1

(AEAT) [2] and Siemens [3] in the absence of radiation. The AEAT Ag–I^- experiments were performed in two batches using (1) Ag powder or (2) Ag mesh, the latter to obtain a better-defined surface area of the Ag sample and to avoid agglomeration of the particles. The Ag–I_2 experiments were performed with Ag mesh. The tests investigate a possible dependence of AgI formation on factors such as pH, temperature, initial iodine concentration and stirring of the test solution. The Siemens experiments investigate the reaction of Ag powder with both I^- and I_2 and cover a wide range of accident-relevant conditions. The influence of pH, temperature, presence of oxygen, initial iodine concentration and stirring of the test solution on the reaction kinetics is studied.

The reaction between I_2 and Ag is found to be very rapid. The rate of stirring has a pronounced effect on the measured rate constants, indicating that mass transfer in the liquid is the rate-controlling step. The uptake of I^- by the Ag mesh surface is slow for test solutions at low pH and even slower at high pH. This is in contrast to the reaction between I^- and Ag powder which is characterised by a rapid, initial drop of the I^- concentration followed by a slower decrease comparable to the one observed in the Ag mesh tests.

3. Model description

Under the experimental conditions described in the previous section AgI is thought to form via a non-catalysed heterogeneous reaction of I^- or I_2 with Ag on the surface of the metallic Ag sample (liquid–solid interface). The overall chemical reactions are formulated as

$$\mathrm{Ag} + \mathrm{I}^- \rightarrow \mathrm{AgI} + \mathrm{e}^- \tag{1}$$

and

$$2\mathrm{Ag} + \mathrm{I}_2 \rightarrow 2\mathrm{AgI}. \tag{2}$$

As the reaction proceeds, an increasing amount of solid AgI is formed on top of the Ag sample acting as a protective layer through which the reactants have to diffuse. We assume the layer to be non-porous as the molar volume of the halide is bigger than that of the metal consumed [5]. In the case of a Frenkel disordered crystal as AgI [6] the disordered fraction of the cations (Ag^+) and electron holes are the diffusing species. The tarnishing reaction proceeds as long as the concentration gradient required for the diffusion of silver ions is maintained. The Ag sample is consumed during the course of the reaction.

It is of interest to investigate the interplay between the chemical reaction rate and the physical transport processes (transport of iodine to the surface of the solid and diffusion of silver through the silver iodide product layer) to be able to derive an expression for the overall conversion rate. We use a resistance-in-series (RIS) model where each of the contributing processes is characterised by a corresponding resistance, defined as the reciprocal of the velocity of the respective process [7,8]. The largest resistance and hence the slowest process controls the overall rate.

3.1. Mass transfer in the liquid and solid

The flux of I^- or I_2 at the reaction interface $r = r_s$ is described by equations derived by means of a film model analysis [7,9]. In this model the mass transfer is proportional to the concentration difference across a stationary film adjacent to the phase boundary. We consider all resistance to mass transfer to be concentrated in this film while in the bulk fluid all composition gradients are eliminated by turbulent mixing. The flux W_A of I^- or I_2 at the particle surface is given by

$$W_A = -\frac{D_I}{\delta}(c_{Ab} - c_{As}) = -k_m(c_{Ab} - c_{As}), \tag{3}$$

where D_I is the diffusion coefficient of I^- or I_2 and δ is the thickness of the stationary liquid film. Since the outer boundary of the liquid film is not known, δ has to be estimated. The bulk and surface concentrations of iodine are given by c_{Ab} and c_{As} (Fig. 1). Estimates of the mass-transfer coefficient k_m will be discussed in Section 3.4. The convection state of the test solution has a significant influence on the thickness of the liquid layer. Stirring results in a decrease of the layer thickness which in turn leads to enhanced mass transfer according to Fick's first law.

The equations governing the flux of Ag^+ towards the reaction interface are derived in analogy to Eq. (3) and hence

$$W_B = k_s(c_{Bb} - c_{Bs}). \tag{4}$$

It can be easily shown that

$$k_{s,sph} = D_s \frac{r_c}{r_s(r_s - r_c)} \tag{5}$$

for spherical particles and

$$k_{s,cyl} = D_s \frac{1}{r_s \ln(r_s/r_c)} \tag{6}$$

for a cylindrically shaped sample. The diffusion coefficient of Ag^+ in AgI is denoted by D_s and the radius of the shrinking particle at time t by r_c, where $r_c(t) \leqslant r_s$ (Fig. 1). The quantities c_{Bb} and c_{Bs} are the Ag^+ concentration at $r = r_c$ and the concentration at the solid–liquid interface $r = r_s$, respectively. The concentration of Ag^+ is assumed to be equal to the Ag concentration. This assumption is, however, only valid if the reaction $\mathrm{Ag} \rightarrow \mathrm{Ag}^+ + \mathrm{e}^-$ proceeds instantaneously at the boundary that separates the Ag and AgI phases and if the rate of the back reaction is negligible.

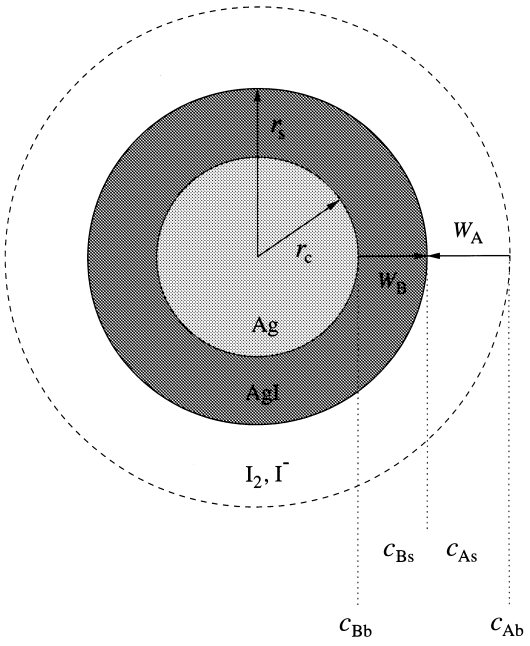

Fig. 1. Schematic representation of the I_2, I^-/AgI/Ag-system with a partially consumed Ag sample (layer thicknesses are not drawn to scale).

3.2. The reaction between Ag and I_2

The reaction between Ag powder or mesh and I_2 will be modelled by means of a 3-RIS model. The reaction scheme consists of the following steps.

(i) Diffusion of the dissolved species A (I_2) through the liquid film adjoining the solid sample to the reaction interface

$$R_{A1} = k_m a_p (c_{Ab} - c_{As}). \tag{7}$$

(ii) Diffusion of species B (Ag^+) through the layer of reacted solid to the reaction interface

$$R_{A2} = k_s a_p (c_{Bb} - c_{Bs}). \tag{8}$$

(iii) Chemical reaction of the dissolved reactant A with the solid species B

$$R_{A3} = k_r a_p c_{As} c_{Bs}, \tag{9}$$

where k_r is the surface reaction rate constant. The chemical reaction is assumed to be first order in both I_2 and Ag to account for the possible depletion of the reactants during the reaction and which allows the coupling of Eqs. (7)–(9).

The quantities R_{Ai}, $i = 1,2,3$, are the rates of change of A in mol/m^3 s and a_p denotes the total surface area of solid per unit volume of liquid (solid–liquid interfacial area), which is given by the (geometrical) surface area of one particle multiplied by the number of particles per unit volume of liquid, n_p, and by a factor f to account for surface roughness effects. For smooth surfaces f is 2–3 whereas for porous, spongy material it can reach 10–1000 [10]. For spherical particles we have $a_p = 4\pi r_s^2 n_p f$; for Ag mesh or wire (cylindrical geometry) we have $a_p = 2r_s \pi L f / V_{sol}$, where we only consider the lateral area of the cylindrical sample. The length of the wire is denoted by L and V_{sol} is the volume of the test solution.

An estimate of the characteristic times of the mass transfer processes and the surface reaction shows that establishment of the steady-state concentration profiles is faster than the change of the overall iodine concentration c_{Ab}. Hence it is justified to assume steady state, where the rates of the contributing processes are equal, $R_{A1} = R_{A2} = R_{A3} = R_A$. This enables us to eliminate the unknown surface concentrations c_{As} and c_{Bs} [11] and yields an expression for the rate of disappearance of A:

$$R_A = \frac{a_p}{2k_r}\left([k_s(k_r c_{Bb} + k_m) + k_m k_r c_{Ab}] - \left\{ [k_s(k_r c_{Bb} + k_m) + k_m k_r c_{Ab}]^2 - 4k_r^2 k_m k_s c_{Ab} c_{Bb} \right\}^{1/2} \right). \tag{10}$$

The rate R_A is equal to the rate of disappearance of B, which for spherical particles is given by

$$R_{B,sph} = \frac{1}{\nu_B}\frac{dc_B}{dt} = \frac{1}{\nu_B}\frac{4\pi}{3}\frac{n_p \rho_B}{M_B}\frac{dr_{c,sph}^3}{dt}, \tag{11}$$

where we have used the identity $R_B = 1/\nu_B \, dc_B/dt$ [10], and ρ_B and M_B are the density and the molecular weight of Ag, respectively. The stoichiometric coefficient of B, ν_B, is given by -2 (Eq. (2)), and Eq. (10) together with Eq. (11) yields

$$\frac{dr_{c,sph}}{dt} = a\left(\frac{r_s}{r_c}\right)^2 \left(\left[\frac{bcr_c}{(r_s - r_c)} + d \right] - \left\{ \left[\frac{bcr_c}{(r_s - r_c)} + d \right]^2 - \frac{ebr_c}{(r_s - r_c)} \right\}^{1/2} \right) \tag{12}$$

with

$$a = -\frac{M_B f}{k_r \rho_B}, \qquad b = \frac{D_s}{r_s}, \qquad c = k_r c_{Bb} + k_m,$$
$$d = k_m k_r c_{Ab}, \qquad e = 4k_r^2 k_m c_{Ab} c_{Bb}. \tag{13}$$

Eq. (12) is integrated numerically by means of a fourth order Runge–Kutta algorithm to obtain a relation between time and r_c. The latter can be related to the fractional conversion $X_{B,sph}(t) = 1 - (r_c/r_s)^3$, which is a measure of how much product C (AgI) has been formed. The mass of C is given by

$$m_{C,sph}(t) = \rho_C \frac{4\pi}{3} r_s^3 X_B \Delta V_M n, \tag{14}$$

where ρ_C is the density of the product C and n the number of particles. The difference of molar volumes

between AgI and Ag is given by $\Delta V_M = M_C\rho_B/(\rho_C M_B)$, where M_C is the molecular weight of AgI. Subsequent division of m_C by the volume of the solution V_{sol} and M_C yields the concentration of C

$$c_C(t) = \frac{m_C(t)}{V_{sol}M_C}. \tag{15}$$

The concentrations of A in the bulk liquid and of B in the bulk solid are gradually depleted as the reaction proceeds, thus c_{Ab} and c_{Bb} are not taken to be constant but become functions of time. They are recalculated at every time-step according to $c_{Ab}(t) = c_{A0} - 1/2c_C(t)$ and $c_{Bb}(t) = c_{B0} - c_C(t)$ making use of the advancement of reaction [10]. Introducing time-dependent bulk concentrations the model becomes quasi-steady state. The quantities c_{A0} and c_{B0} are the I_2 and Ag concentrations at $t = 0$.

For tests with Ag mesh Eqs. (11), (12) and (14) have to be modified slightly to account for the different geometry. With Eq. (6) and

$$R_{B,cyl} = \frac{1}{\nu_B}\frac{\pi L\rho_B}{M_B V_{sol}}\frac{dr_{c,cyl}^2}{dt} \tag{16}$$

we find

$$\frac{dr_{c,cyl}}{dt} = a\frac{r_s}{r_c}\left(\left[\frac{bc}{\ln(r_s/r_c)} + d\right] - \left\{\left[\frac{bc}{\ln(r_s/r_c)} + d\right]^2 - \frac{eb}{\ln(r_s/r_c)}\right\}^{1/2}\right). \tag{17}$$

The fractional conversion is now given by $X_{B,cyl}(t) = 1 - (r_c/r_s)^2$ and the mass of C is determined according to $m_{C,cyl}(t) = \rho_C\pi L r_s^2 X_B \Delta V_M$. Eq. (15) relates m_C to the AgI concentration c_C.

3.3. The reaction between Ag and I^-

As discussed in Section 2 experimental results indicate that the reaction of I^- with Ag involves two processes: an initial, rapid and a long-term, slow reaction. A literature survey [4,12] showed that a significant conversion of I^- and Ag to AgI in aqueous solutions can be observed only under oxidising conditions (presence of oxygen or products of water radiolysis). Supporting evidence is provided by tests performed by AEAT [2] which showed that the degree of oxidation of the Ag surface plays an important role for reactions between I^- and Ag. This suggests that the differences in the extent of the initial, rapid reaction are due to variations in the degree of oxidation of the Ag surfaces that had been used in the experiments. Surface oxidation does, however, not seem to have any effect on the reaction between I_2 and Ag [13].

A layer of silver(I) oxide (Ag_2O) with a thickness of 2–3 nm forms on top of metallic Ag in air already at room temperature [14]. The reaction of I^- with this layer of Ag_2O according to

$$Ag_2O + 2I^- + 2H^+ \rightarrow 2AgI + H_2O \tag{18}$$

would be expected to be rapid and could therefore explain the observed experimental results. Thermochemical calculations suggest that the back reaction is negligible. Diffusion of I^- to the solid surface and subsequent reaction with the silver oxide lead to the formation of AgI on top of the remaining Ag_2O, which continues until the surface oxide initially present has been consumed. We assume that this reaction leaves only patches of AgI on the surface which do not inhibit further diffusion of I^- to the reaction interface. The initial, rapid step of the reaction of I^- with Ag is modelled using a 2-RIS model which incorporates diffusion of I^- to the reaction interface at $r = r_{ox}$:

$$R_{A1} = k_m a'_p(c_{Ab} - c_{As}) \tag{19}$$

and subsequent reaction between I^- and Ag_2O

$$R_{A2} = k_{ox}a'_p c_{As}c_{Db}. \tag{20}$$

The surface reaction rate constant k_{ox} characterises the reaction between I^- and Ag_2O, and c_{Db} is the bulk concentration of Ag_2O. The quantity a'_p is given by $a'_p = 4\pi r_{ox}^2 n_p f$ and $a'_p = 2r_{ox}\pi L f/V_{sol}$ for spherical and cylindrical geometry, respectively, where r_{ox} is the radius of the shrinking solid particle and $r_x \geqslant r_{ox}(t) \geqslant r_s$ (Fig. 2). Under the assumption of a steady state and considering that $R_A = R_D = (1/\nu_D)dc_D/dt$ the same procedure as discussed in Section 3.2 leads to

$$\frac{dr_{ox}}{dt} = -\frac{M_{Ag_2O}}{\rho_{Ag_2O}}c_{Ab}f\left[\frac{1}{k_m} + \frac{1}{k_{ox}c_{Db}}\right]^{-1} \tag{21}$$

for both Ag particles and mesh, where $\nu_D = \nu_{Ag_2O} = -1$ (Eq. (18)). The change of radius can again be related to the fractional conversion of Ag_2O into AgI and hence the total amount of AgI produced. Due to the depletion of the reactants during the reaction the concentrations of I^- and Ag_2O are given by $c_{Ab}(t) = c_{A0} - c_C(t)$ and $c_{Db}(t) = c_{D0} - 1/2c_C(t)$, where c_{D0} is the initial concentration of Ag_2O. The reaction proceeds until all the silver oxide has been consumed.

The transition to the subsequent, slow increase of the AgI concentration occurs when $r_{ox} = r_s$ and it is modelled by means of the 3-RIS model described in Section 3.2. However, instead of Eq. (9) we now use

$$R_{A3} = k'_r a_p \frac{c_{As}c_{Bs}}{c_{A0}c_{B0}} \tag{22}$$

for the chemical reaction at the reaction interface which reproduces the experimentally observed behaviour of the rate for short and long times. The quantity c_{A0} is now the I^- concentration at the beginning of the second, slow

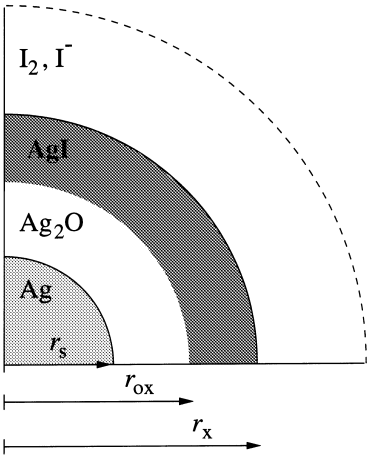

Fig. 2. Schematic representation of the oxidised Ag sample (layer thicknesses are not drawn to scale).

reaction. As already shown before we eliminate the unknown surface concentrations c_{As} and c_{Bs} by assuming steady state. Using $R_A = R_B$ we obtain again Eqs. (12) and (17) but with the new parameters

$$a = -\frac{fM_B k_m}{2\rho_B}, \qquad b = \frac{D_s}{r_s}, \qquad c = \frac{c_{Bb}}{k_m} + \frac{c_{A0}c_{B0}}{k'_r},$$
$$d = c_{Ab}, \qquad e = \frac{4c_{Ab}c_{Bb}}{k_m}, \tag{23}$$

where we have used $\nu_B = -1$ (Eq. (1)).

Due to differences in age and handling of the silver samples the Ag mesh appears to be free from a surface silver oxide layer: the experimental data do not show the initial, rapid step observed for the Ag powder samples but only the slow, long-term step throughout the duration of the experiments. Hence, the reaction between Ag mesh and I^- is modelled by means of the 3-RIS model given by Eqs. (17) and (23).

3.4. Determination of model parameters

The application of the discussed models requires knowledge of the total Ag surface area available for reaction A_{tot} which strongly depends on the particle size distribution, shape and surface roughness effects [10]. BET measurements performed by Siemens for different types of Ag powder show a significant increase of A_{tot} with respect to the geometrical surface area A_{geo}, highlighting the importance of knowing the effective surface area available for reaction [15]. These measurements have, however, been performed prior to the tests and probably overestimate the effective surface area which decreases during the course of the reaction due to agglomeration and settling of the particles. The Ag powder shows a wide range of particle sizes and shapes as demonstrated by scanning electron microscopy examinations performed by AEAT [2]. Due to a lack of data on the particle size distribution and shape we make the simplifying assumption that the powder sample consists of spherical and uniformly shaped particles. The mean particle radius is taken to be 2×10^{-6} m for both AEAT and Siemens tests. However, the combined effects of agglomeration, settling and surface roughness render the determination of A_{tot} difficult. Therefore we use A_{geo} ($f = 1$) for the AEAT powder tests. For the Siemens tests the BET surface area at the beginning of the experiments is known. The mesh sample has a better-defined surface area and hence it is justifiable to assume $f = 1$. The mesh radius is 2.5×10^{-5} m [16].

The thickness of the liquid boundary layer, which is needed to determine the mass-transfer coefficient, is given by $\delta \approx 10^{-5}$ m for well stirred solutions and by $\delta \approx 5 \times 10^{-5}$ to 10^{-4} m for less well stirred solutions [10]. The I^-–Ag experiments were performed with stirring of the test solution although the mesh was less well dispersed in the solution than the powder [16]. Therefore we use $\delta = 5 \times 10^{-5}$ m for modelling the I^-–Ag mesh tests. The diffusivity of I^- in aqueous solutions is given by $D_{I^-} = 2.04 \times 10^{-9}$ m^2/s at $T = 25$°C and $D_{I^-} = 4.5 \times 10^{-9}$ m^2/s at $T = 90$°C [17]. With Eq. (3) we find $k_m \simeq 4 \times 10^{-5}$ m/s and $k_m \simeq 9 \times 10^{-5}$ m/s at $T = 25$°C and $T = 90$°C, respectively. The mass-transfer coefficient for the well stirred powder tests is given by $k_m \simeq 2 \times 10^{-4}$ m/s at $T = 25$°C. The diffusion coefficient of I_2 in aqueous solutions is smaller than D_{I^-} which is consistent with the size and molecular weight of the species involved. It is given by $D_{I_2} = 1.36 \times 10^{-9}$ m^2/s at $T = 25$°C [18]. Estimating the mass-transfer coefficient as discussed above we obtain $k_m \simeq 10^{-4}$ m/s for stirred I_2–Ag tests and $k_m \simeq 10^{-5}$ m/s for static experiments. This is in agreement with the measured pseudo-first order rate constants [2] indicating that the rate is determined by k_m. The exact values of k_m are obtained numerically by fitting the model to the experimental data. The arithmetic mean of the mass-transfer coefficient for a series of experimental sets at 25°C has been determined to $\overline{k}_m = (2.2 \pm 0.6) \times 10^{-5}$ m/s for static tests and $\overline{k}_m = (1.6 \pm 0.2) \times 10^{-4}$ m/s for tests with rapid stirring of the test solution. The uncertainty is one standard deviation. Due to the scarcity of experimental data the I_2–Ag reaction at $T = 90$°C could not be analysed quantitatively.

The diffusion coefficient of Ag^+ in AgI is given by

$$D_s = D_0 \exp(-E/RT) \tag{24}$$

with the parameters $D_0 = 3 \times 10^{-5}$ m^2/s, $E = 59433$ J/mol for β-AgI (hexagonal) and $D_0 = 5 \times 10^{-8}$ m^2/s, $E = 35576$ J/mol for γ-AgI (fcc) [19]. The quantity R is the ideal gas constant and T is the temperature in K. Under standard conditions both modifications of AgI are stable and coexist [20]. As a conservative estimate we use the smaller diffusivity of Ag^+ in β-AgI for our cal-

culations. We find $D_s = 1.2 \times 10^{-15}$ m^2/s at $T = 25$°C and $D_s = 8.5 \times 10^{-14}$ m^2/s at $T = 90$°C.

A sensitivity analysis of the model predictions for I^-–Ag mesh reactions and for the slow step of the powder tests shows that the model is sensitive to even minor changes of the reaction rate constant k_r'. This suggests that the reaction is not limited by mass transfer in the liquid but by the chemical reaction at the reaction interface. With the given set of parameters k_r' is the only free parameter and is determined by fitting the model to the experimental data. At 25°C we obtain $\overline{k}_r' = (8.2 \pm 3.6) \times 10^{-9}$ mol/m^2 s based on AEAT powder/mesh tests as well as on Siemens powder experiments, where no clear pH dependence of the rate can be observed. At 90°C and at pH = 4.6, $\overline{k}_r' = (3.4 \pm 1) \times 10^{-8}$ mol/m^2 s is obtained decreasing to $\overline{k}_r' = (7.3 \pm 1.5) \times 10^{-9}$ mol/m^2 s at pH = 7. The rate of the I_2–Ag experiments is controlled by mass transfer in the liquid. A lower boundary value for k_r is determined in analogy to the I^-–Ag experiments by a sensitivity analysis. We find $k_r \gtrsim 2 \times 10^{-4}$ m^4/mol s. A summary of estimated and fitted model parameters is given in Table 1.

The initial, rapid step of the reaction of I^- with Ag powder is characterised by the surface reaction rate constant k_{ox}. The value of k_{ox} that reproduces the initial, steep rise of the rate is determined by numerical experiments, yielding $\overline{k}_{ox} = (2.2 \pm 1.7) \times 10^{-3}$ m^4/mol s.

Information on the initial silver oxide concentration c_{D0} is not available from the experiments. However, this quantity limits the maximum amount of AgI that can be produced by reaction of I^- with the Ag_2O layer (Eq. (18)). Hence it determines when the transition from the initial, rapid to the subsequent, slow reaction takes place, which provides a means to estimate c_{D0}. This procedure yields a degree of surface oxidation that ranges from 0.1 to 0.2% of the Ag mass for the AEAT experiments to 0.7% for the Siemens tests. The initial concentration of Ag_2O depends solely on how the Ag sample was handled prior to the test.

4. Discussion and conclusions

The reaction of I^- or I_2 with either particulate Ag or mesh in the LWR containment sump has a major impact on iodine volatility from solution. These reactions have been modelled under quasi-steady-state conditions by means of resistance-in-series models which incorporate transport phenomena and a chemical reaction. The model was validated successfully against separate-effects tests over a variety of conditions. The application of the model requires knowledge of the total surface area available for reaction. It is a function of the combined effects of agglomeration, settling and surface roughness for particulate Ag and therefore difficult to estimate. An area of remaining uncertainty is the extent of oxidation of the Ag surface which plays a decisive role for reactions between I^- and Ag.

Both stirred and static experiments for I_2–Ag reactions seem to be limited by diffusion in the bulk liquid. This is probably due to the smaller diffusion coefficient of I_2 in aqueous solutions compared to I^- and the fast chemical reaction at the surface (Fig. 3). The experimental finding that the overall rate of formation of silver iodide is independent of the number of accumulated monolayers of AgI can be explained by the fact that diffusion in the AgI layer appears not to be rate controlling. Hence, for the duration of the experiment the overall reaction rate does not follow a parabolic law as is usually the case for tarnishing reactions. The model overpredicts the rate in the case of the Siemens tests (Fig. 4). This is thought to be due to agglomeration or settling of the particles during the test which will decrease the effective surface area and hence the rate. This effect is not taken into account in our model.

The degree of oxidation of the Ag surface seems to play a decisive role for reactions between I^- and Ag. The initial concentration of Ag_2O determined for each experimental set corresponds to the expected thickness of a silver oxide layer that forms on top of metallic Ag in air

Table 1
Estimated and fitted model parameters

	Mass-transfer coefficient	Reaction rate constant
I_2 + Ag:	$\overline{k}_m$ in 10^{-5} m/s [a]	
Static (25°C)	2.2 ± 0.6	$\overline{k}_r \gtrsim 2 \times 10^{-4}$ m^4/mol s [a]
Rapid stirring (25°C)	16 ± 2	As above
I^- + Ag:	$\overline{k}_m$ in 10^{-4} m/s [b]	$\overline{k}_r'$ in 10^{-9} mol/m^2 s [a]
Powder (25°C)	2	8.2 ± 3.6
Mesh (25°C)	0.4	As above
Mesh (90°C, pH = 4.6)	0.9	34 ± 10
Mesh (90°C, pH = 7)	As above	7.3 ± 1.5

[a] Fitted model parameters.
[b] Estimated model parameters.

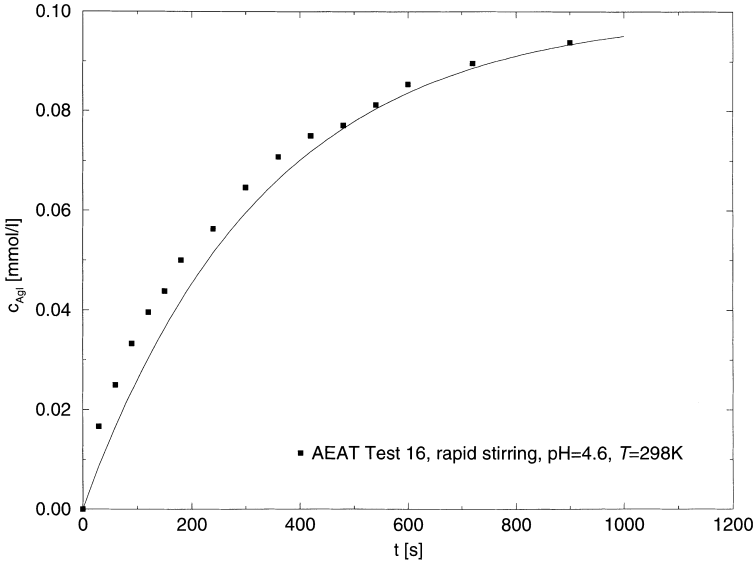

Fig. 3. RIS model predictions (solid line) for the reaction of I_2 with Ag mesh compared to experimental data (solid squares). The calculations were performed with the mean values of the rate constants ($c_{A0} = 5 \times 10^{-5}$ mol/l, $m_{Ag} = 126$ mg, $V_{sol} = 50$ cm^3).

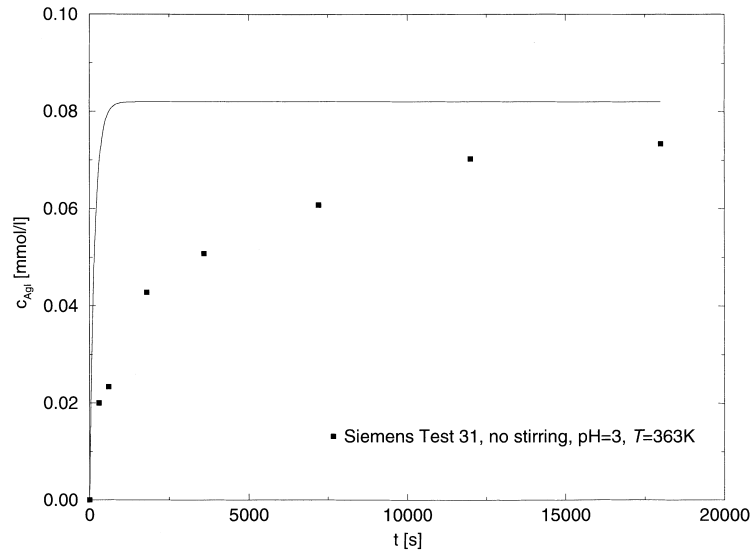

Fig. 4. Comparison of model predictions for the I_2–Ag powder reaction with experimental data ($c_{A0} = 4 \times 10^{-5}$ mol/l, $m_{Ag} = 1$ g, $V_{sol} = 1$ l).

at room temperature [14]. The initial, rapid step is limited by the depletion of the oxide layer; mass transfer in the liquid, however, contributes to the reaction rate. The slow reaction between I^- and Ag mesh as well as the second, slow step of the Ag powder experiments are limited by the chemical reaction at the liquid–solid boundary. Model predictions are influenced by k_r' alone whereas changes of D_s and k_m have practically no effect on the rate. The gradual transition from the rapid to the slow stage of the Siemens tests is not predicted by our model (Fig. 5). This is thought to be due to effects such as agglomeration, formation of AgI colloids and changes in mass transfer conditions which are specific to the conditions under which the tests were performed [21] and which we have neglected in our studies. The I^-–Ag mesh rate does not show the initial, rapid step as observed for the I^-–Ag powder reaction (Fig. 6). This suggests that the mesh surface was not as extensively

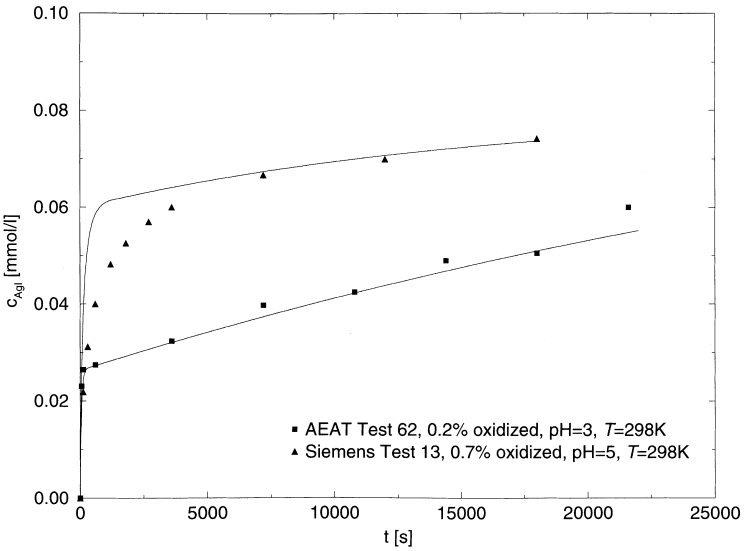

Fig. 5. RIS model simulations of I^-–Ag powder tests compared to experimental results (Test 62: $c_{A0} = 10^{-4}$ mol/l, $m_{Ag} = 1.41$ g/l, $V_{sol} = 0.1$ l; Test 13: $c_{A0} = 8 \times 10^{-5}$ mol/l, $m_{Ag} = 1$ g, $V_{sol} = 1$ l).

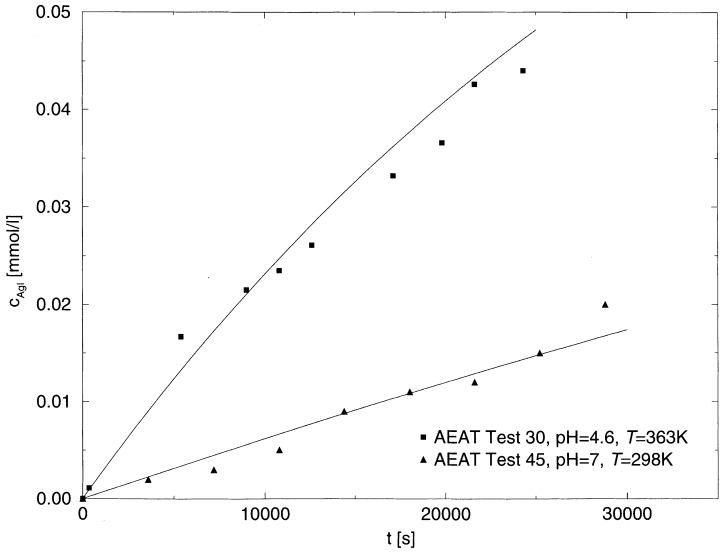

Fig. 6. Model predictions of the reaction between I^- and Ag mesh for different pH and temperature ($c_{A0} = 10^{-4}$ mol/l, $m_{Ag} = 10$ g/l, $V_{sol} = 0.1$ l).

oxidised as the Ag powder which can be explained by different preparation routes, ages and storage conditions of the Ag samples [2]. At high pH (>7) and in the absence of oxidising conditions the I^-–Ag reaction is so slow as to probably be negligible.

Simulations of tests performed in the presence of radiation have been carried out with the mechanistic iodine chemistry code INSPECT [22]. Inclusion of a simplified version of the resistance-in-series models discussed herein was found to greatly improve agreement between test results and model predictions [21]. This encourages incorporation of the proposed model into severe accident iodine codes.

The proposed resistance-in-series model can be easily extended to reactions in the gas phase. Work is underway to determine the amount of AgI that could

be formed by the possible reaction between Ag aerosols and gaseous iodine in the containment atmosphere.

Acknowledgements

The authors would like to thank Dr S. Dickinson from AEA Technology and Dr F. Funke from Siemens KWU for stimulating discussions and for providing the data from their experimental work. The first author thanks the European Commission for awarding her a Marie Curie Fellowship.

References

[1] C.A. Chuaqui et al., Phebus Report PH-PF IP/96/300 (1996).
[2] P. Cake, S. Dickinson, Kinetic studies of the reaction of aqueous iodine with silver surfaces, AEAT-1547 (1997).
[3] F. Funke, G.-U. Greger, A. Bleier, S. Hellmann, W. Morell, The reaction between iodine and silver under severe PWR accident conditions – An experimental parameter study, in: Proceedings of Fourth CSNI Workshop on the Chemistry of Iodine in Reactor Safety, Würenlingen, Switzerland, 10–12 June 1996.
[4] D. Jacquemain, C. Poletiko, C.A. Chuaqui, Phebus Report PH-PF IP/96/303 (1996).
[5] A.W. Adamson, Physical Chemistry of Surfaces, Interscience, New York, 1960.
[6] N.B. Hannay, Solid-State Chemistry, Prentice-Hall, Englewood Cliffs, NJ, 1967.
[7] M.M. Clark, Transport Modelling for Environmental Engineers and Scientists, Wiley/Interscience, New York, 1996.
[8] K.R. Westerterp, W.P.M. van Swaaij, A.A.C.M. Beenackers, Chemical Reactor Design and Operation, Wiley, New York, 1987.
[9] R. Taylor, R. Krishna, Multicomponent Mass Transfer, Wiley, New York, 1993.
[10] G.W. Castellan, Physical Chemistry, third edition, Addison-Wesley, Reading, MA, 1983.
[11] L.K. Doraiswamy, M.M. Sharma, Heterogeneous Reactions: Analysis, Examples and Reactor Design, vol. 2: Fluid–Fluid–Solid Reactions, Wiley, New York, 1984.
[12] S. Hellmann, G.-U. Greger, F. Funke, A. Bleier, Theoretische und experimentelle Untersuchungen zum Verhalten des Jods bei auslegungsüberschreitenden Ereignissen: Organojod, Jod/Silber-Reaktion, Jod/Eisen-Reaktion, teil 1: Literaturstudien, Abschlußbericht BMFT Fördervorhaben 1500 823 (1992).
[13] G. Cohn, Chem. Rev. 42 (1948) 527.
[14] Gmelins Handbuch der Anorganischen Chemie, 8. Auflage, Silber, teil B1, Verlag Chemie, Weinheim, 1971.
[15] G.-U. Greger, F. Funke, A. Bleier, S. Hellmann, M. Beuerle, Theoretische und experimentelle Untersuchungen zum Verhalten des Jods bei auslegungsüberschreitenden Ereignissen: Organojod, Jod/Silber-Reaktion, Jod/Eisen-Reaktion, teil 3: Jod/Silber-Reaktion, Abschlußbericht BMFT Fördervorhaben 1500 823 (1995).
[16] S. Dickinson, private communication.
[17] D.R. Lide (Ed.-in-Chief), Handbook of Chemistry and Physics, 76th edition, CRC Press, Boca Raton, 1995/1996.
[18] L. Cantrel, R. Chaouche, J. Chopin-Dumas, J. Chem. Eng. Data 42 (1997) 216.
[19] P. Jordan, M. Pochon, Helv. Phys. Acta 30 (1957) 33.
[20] Gmelins Handbuch der Anorganischen Chemie, 8. Auflage, Silber, teil B2, Verlag Chemie, Weinheim, 1972.
[21] S. Dickinson, Modelling of iodine–silver reactions, AEAT-2094 (1) (1997).
[22] W.G. Burns, H.E. Sims, in: A.C. Vikis (Ed.), Proceedings of Second CSNI Workshop on Iodine Chemistry in Reactor Safety, AECL-9923, CSNI-149, 1989.